ELSEVIER

PII: S0954-1810(97)00003-4

Artificial Intelligence in Engineering 11 (1997) 413–419

Printed in Great Britain
0954-1810/97/$17.00

Extraction of structures from turbulent signals

J. Ferre-Gine,[a] R. Rallo,[a] A. Arenas[a] & Francesc Giralt[b]

[a]*Departamento d'Enginyeria Informàtica,* [b]*Departament d'Enginyeria Química, Escola Tècnica Superior d'Enginyeria, Universitat Rovira i Virgili, 43006 Tarragona, Catalunya, Spain*

(Received for publication 6 January 1997)

An automatic procedure based on of the Fuzzy ARTMAP neural network is applied to classify the structure embedded in two-component velocity signals measured in a turbulent wake behind a circular cylinder. A small part of the velocity field in the horizontal plane of the wake recorded at two downstream positions $x/D = 30$ and 150 was pre-processed to extract a set of relevant patterns from the data in order to train the network. The complete data files were tested with the trained net, obtaining nine different structures: clockwise and anti-clockwise eddies, sinks, sources, four types of saddle points and jet-like motions. Comparison of the number of classes and patterns belonging to the same category at at $x/D = 30$ and 150 shows that the number of structures present in the wake increase with downstream position, i.e. with the development of turbulence. The jets present in the near wake appear in this preliminary analysis to be linked to the formation of double rollers in the far wake. © 1997 Elsevier Science Limited.

Key words: turbulent wake, fuzzy artmap, coherent structures.

1 INTRODUCTION

The study of the coherent structures embedded in turbulent flows is important to understand the dynamics and the transfer processes of momentum, heat and mass in most flows of engineering interest. Also, the automatic and continuous monitoring and identification of the structures present in such flows could be used to control turbulence.

Turbulent wakes and shear layers have been the object of experimental and numerical analysis since the studies of Townsend[1], Grant[2] and Brown and Roshko[3] showed the dominant effects of large scale coherent motions in these turbulent flows. To understand the development of turbulence in the wake behind a circular cylinder and the role played by coherent structures it is useful to relate the near wake, where the flow is quasi-two-dimensional and dominated by Kármán vortices shed parallel to the cylinder axis, with the far wake where the flow is fully turbulent.

The most commonly used methods to identify coherent motions are flow visualisation, spectral and correlation analysis, principal component analysis or proper orthogonal decomposition, conditional sampling and pattern recognition with template matching and linear stochastic estimates. Most of the analytical techniques mentioned above are capable to detect and identify statistically significant structures in a global or averaged framework. They may present, however, difficulties when local recognition and classification are required. The application of artificial intelligence and neural networks to structure identification can provide the basis for unbiased pattern recognition and classification of locally occurring structures in turbulent flows.

In this paper, an implementation of the Fuzzy ARTMAP Neural Network[4] capable of identifying eddy motions in two-dimensional velocity fields of a turbulent flow[5] is applied to characterise the structural evolution of a turbulent wake flow with downstream position. The automatic procedure is applied to locally classify the different structures and motions embedded in two component velocity signals sensed in the near ($x/D = 30$) and far ($x/D = 150$) regions of the wake. A pre-processing procedure, based on the geometric characteristics of the set of vectors representing an eddy motion, is used to pre-classify vortex-like patterns before data are presented to the net to obtain the training set. Data measured by Professor Antonia at the University of Newcastle (Australia) in the far wake region have been used to train the network. The trained network is applied to analyse the data measured in Tarragona[6,7] at two downstream positions $x/D = 30$ and 150. Comparison between the classes at these two locations shows the effect of the evolution from a nearly two-dimensional flow in the near wake to a three-dimensional turbulent wake flow further downstream.

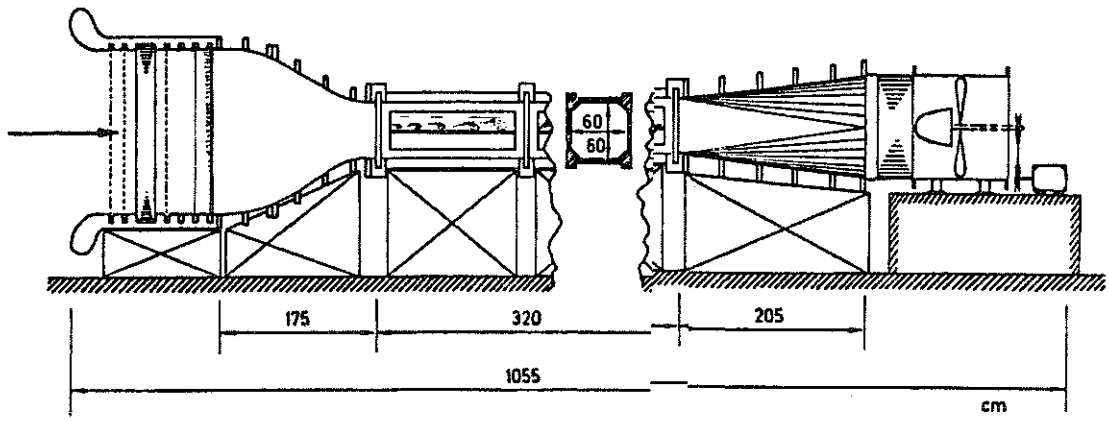

Fig. 1. Sketch of the low turbulence wind tunnel.

2 THE EXPERIMENT

The two-component velocity data analysed here by Pons[6] and Vernet *et al.*[7] were measured in a wake behind a circular cylinder ($D = 3{\cdot}25$ mm) at $Re = DU_0/n = 1600$ ($U_0 = 7{\cdot}8$ m/s). Briefly, the flow was generated in the low turbulence wind tunnel of Tarragona (see Fig. 1) with a test section 60 × 60 cm square and 3 m long. An array of five X-wire probes (8 DISA 55M10 and 2 DISA 56C17 anemometers) was placed at the horizontal central plane of the wake at $x/D = 30$ and 150 (see Fig. 2). Voltage signals from the anemometers were low-pass filtered and digitised at 4 kHz per channel during 30 s. Data were stored and processed in a HP Apollo 730 to obtain files of the u-component (x-direction or flow direction) and w-component (z-direction or spanwise coordinate) of the velocity field. The analysis presented in this work of these two-component u and w data measured simultaneously at five spanwise z locations separated 30 mm in the horizontal plane was carried out on a CRAY YMP-EL computer.

3 THE ARTMAP SYSTEM AND DATA PRECONDITIONING

A supervised Fuzzy ARTMAP neural network[4,5] is used to identify eddy motions present in the horizontal (homogeneous) spanwise direction of a turbulent wake flow. The Fuzzy ARTMAP neural network is powerful

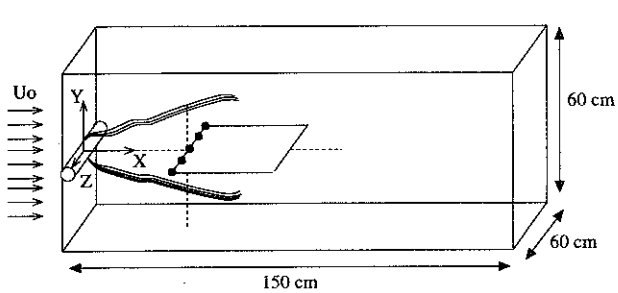

Fig. 2. Arrangement of probes.

in difficult classification problems. It is based on the adaptive resonance theory, which avoids the so called stability–plasticity dilemma. A Fuzzy ARTMAP neural network consists of a pair of Fuzzy[8] modules, art_a and art_b, linked by an associative memory and an internal controller. The controller is designed to create the minimal number of categories (or hidden units) to meet accuracy criteria. This is done by implementing a learning rule that minimises predictive error and maximises generalisation.

The present implementation forces the art_b module to have only one category representing clockwise eddies (see CE in Fig. 3). Another fictitious category considered is the one corresponding to the 'I do not know' answer by the net. All inputs that do not pass the reset process of classification, for a given vigilance parameter ρ, i.e. that do not match with any structure, are included in this category and considered not to be eddy motions. A representation of this net is presented in Fig. 4. Each fuzzy subsystem art_a and art_b includes a field of nodes F_0 which represents a current input vector $\mathbf{F}_1$. This vector $\mathbf{F}_1$ receives both bottom-up input from F_0 and top-down input from a field F_2, which represents the active code or category. The activity vectors $\mathbf{F}_1$ and $\mathbf{F}_2$ are denoted by $\mathbf{x} = (x_1, \ldots, x_M)$, and $\mathbf{y} = (y_1, \ldots, y_M)$, respectively. The number of nodes in each field is arbitrary. Associated with each F_2 category node j ($j = 1, \ldots, N$) there is a vector $\mathbf{w}_j = (w_{j1}, \ldots, w_{jM})$ of adaptive weights. Initially, when each category is said to be uncommitted, $w_{j1} = \cdots = w_{jM} = 1$. After a category is selected for coding it becomes committed.

The dynamics of fuzzy ART are determined by a choice parameter $\alpha > 0$, a learning rate parameter $\beta \in [0, 1]$, and a vigilance parameter $\rho \in [0, 1]$.

For each input $\mathbf{I}$ and F_2 node j, the *choice function* T_j is defined by

$$T_j(\mathbf{I}) = \frac{|\mathbf{I} \wedge \mathbf{w}j|}{\alpha + |\mathbf{w}j|}. \tag{1}$$

In eqn (1) the fuzzy AND operator ($\wedge$) is defined by

$$(\mathbf{p} \wedge \mathbf{p}) = \min(p_i, q_i) \tag{2}$$

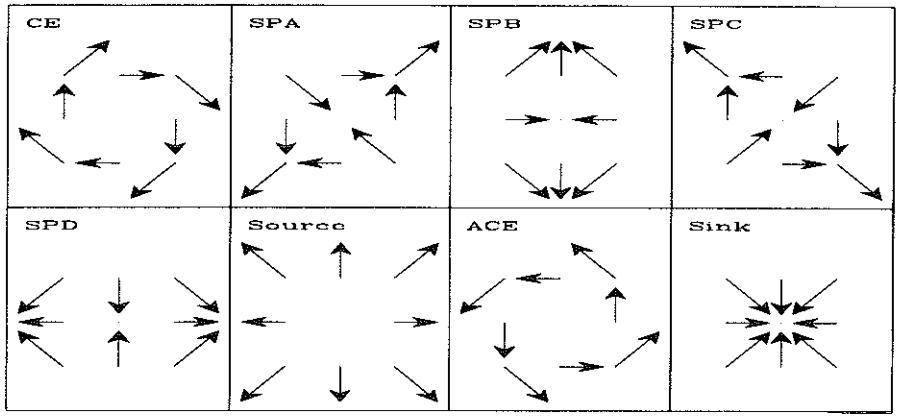

Fig. 3. Transformations of a clockwise eddy (CE) into a saddle point A.D (SPA.SPD), source, anticlockwise eddy (ACE) and sink.

and the norm $|.|$ by

$$|\mathbf{p}| = \sum_{i=0}^{M} |p_i| \tag{3}$$

for any M-dimensional vectors $\mathbf{p}$ and $\mathbf{q}$. For simplicity, $T_j(\mathbf{I})$ is written as T_j when the input $\mathbf{I}$ is fixed.

The system is said to make a *category choice* when at most one F_2 node can become active at a given time. The category choice is indexed by J, where

$$T_J = \max\{T_j : j = 1, \ldots, N\}. \tag{4}$$

When the Jth category is chosen, $y_J = 1$, and $y_J = 0$ for $j \neq J$.

In a choice system, the F_1 activity vector $\mathbf{x}$ is characterised by the equation:

$$\mathbf{x} = \begin{cases} \mathbf{I} & \text{if } F_2 \text{ is inactive} \\ \mathbf{I} \wedge \mathbf{w}_J & \text{if the } J\text{th } F_2 \text{ node is chosen.} \end{cases} \tag{5}$$

Resonance occurs if the match function $|\mathbf{I} \wedge \mathbf{w}_J|/|\mathbf{y}|$ of the chosen category meets the vigilance criterion

$$\frac{|\mathbf{I} \wedge \mathbf{w}_J|}{|\mathbf{I}|} \geq \rho. \tag{6}$$

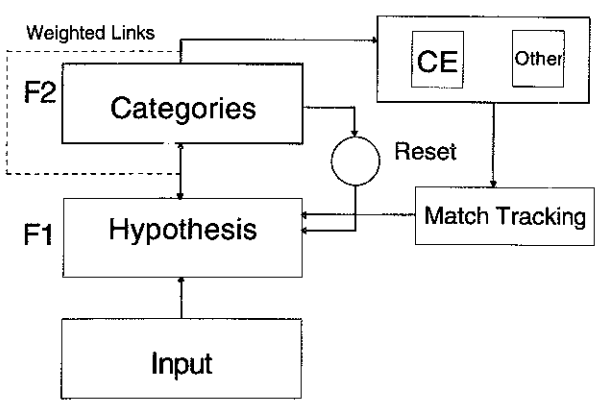

Fig. 4. Sketch of the Fuzzy ARTMAP system.

When Jth category is chosen, resonance occurs if

$$|\mathbf{x}| = |\mathbf{I} \wedge \mathbf{w}_J| \geq \rho|\mathbf{I}|. \tag{7a}$$

Learning then ensues, as defined below. Mismatch reset occurs if

$$\frac{|\mathbf{I} \wedge \mathbf{w}_J|}{|\mathbf{I}|} \leq \rho \tag{7b}$$

and then a new index $\mathbf{J}$ is chosen. The search process continues until the chosen J category meets the vigilance criterion (6). Once the search ends, the weight vector $\mathbf{w}_J$ is updated according to

$$\mathbf{w}_J^{(\text{new})} = \beta(\mathbf{I} \wedge \mathbf{w}_J^{(\text{old})}) + (1 - \beta)\mathbf{w}_J^{(\text{old})} \tag{8}$$

where fast learning corresponds to $\beta = 1{\cdot}0$.

The modules art_a and art_b are linked via an inter-ART module, F^{ab}, called a map field. Inputs to art_a and art_b are $\mathbf{I} = \mathbf{A}$ and $\mathbf{I} = \mathbf{B}$, respectively. Variables in art_a or art_b are designated by superscripts a or b. In the former case, $\mathbf{x}^a = (x_1^a, \ldots, x_{2M_a}^a)$ denotes the F_1^a output vector, $\mathbf{y}^a = (y_1^a, \ldots, y_{2N_a}^a)$ the F_2^a output vector, and $\mathbf{w}_j^a = (w_{j,1}^a, \ldots w_{j,2M_a}^a)$ the jth art_a weight vector. For art_b $\mathbf{x}^b = (x_1^b, \ldots, x_{2M_b}^b)$ denotes the F_1^b output vector, $\mathbf{y}^b = (y_1^b, \ldots, y_{2N_b}^b)$ the F_2^b output vector, and $\mathbf{w}_k^b = (w_{k,1}^b, \ldots, w_{k,2M_b}^b)$ the kth art_b weight vector. For the map field $\mathbf{x}^{ab} = (x_1^{ab}, \ldots, x_{N_b}^{ab})$ denotes the F^{ab} output vector, and $\mathbf{w}_j^{ab} = (w_{j1}^{ab}, \ldots, w_{j2N_b}^{ab})$ the weight vector from the jth F_2^a node to F^{ab}. Initially, each weight is set equal to 1.

The map field F^{ab} is activated when one of the art_a or art_b categories becomes active. When the jth F_2^a node is chosen, the input $F_2^a \rightarrow F^{ab}$ is proportional to the weight vector $\mathbf{w}_j^{ab}$. When the kth F_2^b is chosen, the F^{ab} node K is activated by 1-to-1 pathways between F_2^b and F^{ab}. If both art_a and art_b are active, as in supervised learning, then F^{ab} activity reflects the degree to which a correct prediction has been made. With fast learning, F^{ab} remains active only if art_a predicts the same category as art_b, via the weight vector $\mathbf{w}_J^{ab}$, or if the active art_a category has not yet learned an art_b prediction. In summary, the F^{ab} output vector $\mathbf{x}^{ab}$ obeys the following

equation:

$$\mathbf{x}^{ab} = \begin{cases} \mathbf{y}^b \wedge \mathbf{w}_J^{ab} & \text{if the } J\text{th } F_2^a \text{ node is active and } F_2^b \text{ is active} \\ \mathbf{w}_J^{ab} & \text{if the } J\text{th } F_2^a \text{ node is active and } F_2^b \text{ is inactive} \\ \mathbf{y}^b & \text{if } F_2^a \text{ is active and } F_2^b \text{ is active} \\ \mathbf{0} & \text{if } F_2^a \text{ is active and } F_2^b \text{ is inactive.} \end{cases} \tag{9}$$

If the prediction $\mathbf{w}_J^{ab}$ is disconfirmed by $\mathbf{y}^b$, this mismatch triggers an art_a search for a new category, as follows. At the start of each input presentation, the art_a vigilance parameter ρ_a equals a baseline vigilance $\bar{\rho}_a$. The map field vigilance parameter is ρ_{ab}. Match tracking is triggered by a mismatch at the map field F^{ab},

$$|\mathbf{x}^{ab}| < \rho_{ab}|\mathbf{y}^b| = \rho_{ab} \tag{10}$$

Match tracking increases ρ_a until it becomes slightly larger than the art_a value, $|\mathbf{A} \wedge \mathbf{w}_J^a||\mathbf{A}|^{-1}$. After match tracking,

$$|\mathbf{x}^a| = |\mathbf{A} \wedge \mathbf{w}_J^a| < \rho_a|\mathbf{A}| = \rho_a \mathbf{M}_a \tag{11}$$

and the art_a search leads to ARTMAP resonance, when a newly chosen F_2^b node J satisfies both the art_a matching criterion

$$|\mathbf{x}^a| = |\mathbf{A} \wedge \mathbf{w}_J^a| \geq \rho_a|\mathbf{A}| \tag{12}$$

and the map field matching criterion

$$|\mathbf{x}^{ab}| = |\mathbf{y}^b \wedge \mathbf{w}_J^{ab}| \geq \rho_{ab}|\mathbf{y}^b|. \tag{13}$$

Otherwise, no such F_2^b node exists and the ART search leads to the shutdown of F_2^b for the remainder of the input presentation. Since $w_{ij}^a(0) = w_{jk}^a(0) = 1$ and $0 \leq \rho_a$, $\rho_{ab} \leq 1$, ARTMAP resonance always occurs if J is an uncommitted node.

A learning rule determines how the map field weights $\mathbf{w}_{jk}^{ab}$ change through time. During resonance with the art_a category J active, $\mathbf{w}_J^{ab}$ approaches the map field vector $\mathbf{x}^{ab}$. With fast learning, once J learns to predict an art_b category K, that association becomes permanent, i.e. $w_{JK} = 1$ and $w_{JK} = 0 (k \neq K)$ for all times. After presentation of all training samples, the net is ready to undergo a test phase to show the accuracy of the created categories.

In the present study the net was trained for six values of the vigilance parameter in the range 0·9–0·95, obtaining a set of weights for each one. Each of the six trained nets was given, during a test phase, all the possible frames obtained from the full data file, so that the frames containing a recirculation could be classified.

A modification of the learning rule was used in this implementation of the Fuzzy ARTMAP neural network. In fast learning, after an association intra-modules was established, weights in both ART modules were updated by the rule

$$\mathbf{w}_J^{new} = (\min(I_1, w_{J_1}^{old}), \ldots, \min(I_N, w_{J_N}^{old})) \tag{14}$$

where J is the committed category. If the vigilance parameter is $\rho = 1{\cdot}0$ the previous rule (14) becomes

$$\mathbf{w}_J^{new} = \mathbf{I} \tag{15}$$

where I is the presented pattern, and the number of categories equals the number of inputs.

Equation (15) with $\rho < 1{\cdot}0$, has been used here in the present implementation of the net. This rule has the effect of partitioning the training set in a manner that each partition class contains those input patterns committing to the same category. The net becomes stable in the sense that the partition is stable between two consecutive presentations of the training set, even if the order of the patterns is altered. However, the weights will depend on the last pattern committed to the category. This is consistent with the formation of categories because the patterns committing to the same category are very similar.

The pre-processing of data followed in the present study is explained in detail elsewhere.[5] Briefly, the velocity field is first transformed into a field of fluctuating velocities with zero mean. These fluctuations are the ones analysed here. Frames F of 3×3 consecutive velocity vectors were considered, and clockwise eddy patterns (CE) were identified by visual observation of the initial 1000 consecutive u and w velocity data measured at five locations in the

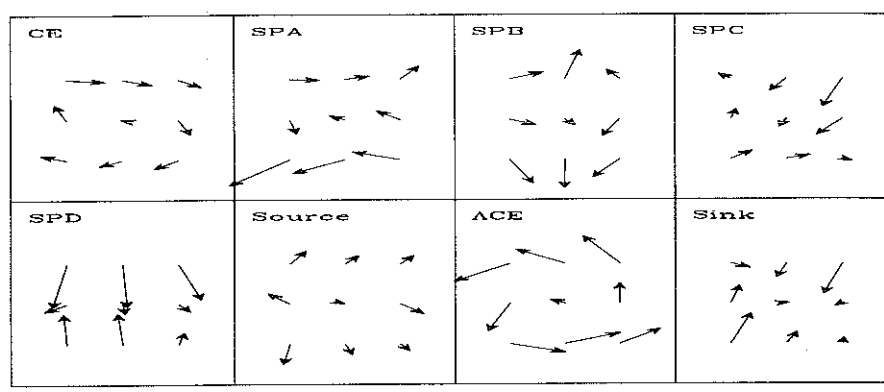

Fig. 5. Samples of structures extracted in the wake behind a circular cylinder at $x/D = 30$ and 150.

Table 1. Total number of structures classified

Type	$x/D = 30$	$x/d = 150$
	Classified structures	
CE	443	617
ACE	506	583
SPA	287	239
SPB	248	395
SPC	311	276
SPD	267	509
Sink	126	121
Source	138	115

z-direction. A filter was designed to automate this identification procedure using the angular components of the vectors forming the eddy patterns. These CE were used to train the net. Finally, the remaining data were passed through the net and CE motions were extracted.

The net also performed well for other kinds of structures, e.g. anticlockwise eddies (ACE), but the method is time consuming. Ferre-Gine *et al.*[5] suggested a method to simplify the time required for extracting additional structures such as the ACE, four types of saddle points (SPs), and the sources and sinks depicted in Fig. 3. This method uses the fact that each of these structures can be obtained by applying to the vectors of a CE-skeleton one of the components of the group of movements leaving invariant a square.[9] The result of these transformations when applied locally to each one of the vectors conforming one CE is given in Fig. 3. Therefore, the net is trained only once to extract the eight type of structures given in Fig. 3.

4 RESULTS AND DISCUSSION

Figure 5 shows samples of patterns pertaining to eight classes of structures extracted from both the near and far wake data measured in Tarragona with five X-wire probes located in the z-direction. Table 1 includes the total number of structures contained in each of these classes over 30 s of recorded data, i.e. the number of 3×3 structures centred at the three central measuring z-locations. The results in this table indicate that the wake flow at $x/D = 30$, while dominated by Kármán vortices, already contains the basic structures found in the turbulent far region at $x/D = 150$.

Table 1 also shows that the number of CE, ACE and total saddle points increase from $x/D = 30$ to 150, as the flow becomes fully turbulent and three-dimensional. The number of saddle points identified at $x/D = 30$ is approximately 70% of the number of Kármán vortices contained in the signal. This percentage is in agreement with the 80% reported by Zhou and Antonia[10] at $x/D = 20$ using critical-point theory. In addition, we have verified that in every frame where Giralt and Ferré[11] confirm, with template matching, a double roller or a pair of counter-rotating eddies, the net classifies two 3×3 frames located nearly side by side in the spanwise direction of the wake, one with a clockwise and the other with anticlockwise eddy. Also present results are in agreement with those reported by Kopp *et al.*[12] using pattern recognition and orthogonal decomposition.

The increase in CE and ACE observed in Table 1 as the flow becomes fully turbulent ($x/D = 150$) is related to the fact that these vortical motions or eddies in the x–z plane are capable of extracting energy from the mean flow by stretching along the x–y plane of the wake, i.e. the plane perpendicular to the z-direction where the probes are located. The CE and ACE can be sustained and grow as vortical motions in the x–z plane due to their simultaneous projection towards the edges of the wake (stretching) in a spiralling motion that contributes to the lateral spread of the wake (y-direction in Fig. 2). This is consistent with the results reported by Giralt and Ferré.[1]

The total number of sinks and sources, i.e. of structures that could be linked to vertical motions across or towards the horizontal plane in the y-direction, remains approximately constant with downstream position due to the fact that Kármán vortices are already three-dimensional at $x/D = 30$. These vertical motions associated with sinks and sources at $x/D = 30$ are linked to Kármán vortices and, thus, should have a significant streamwise velocity component in the direction of the flow, giving rise to 'jet-like' motions in the horizontal x–z plane of the fluctuating velocity field. In fact, the occurrence of side-by-side jets in this plane with opposing fluctuating motions would generate vorticity in the perpendicular y-direction which by stretching would grow into CEs and ACEs further downstream, explaining the increase in these structures with increasing x/D, observed in Table 1.

Table 2 includes the number of jet-like structures identified in the x–z plane at $x/D = 30$ and 150. Three different types of jets motions have been considered: (i) jets spanning three sensors and with u velocities

Table 2. Number of jets classified

	9°		18°		27°	
	$x/D = 30$	$x/D = 150$	$x/D = 30$	$x/D = 150$	$x/D = 30$	$x/D = 150$
Jets (i)	12	10	186	110	605	421
Jets (ii)	14	18	142	220	524	723
Jets (iii)	489	361	2876	2412	7064	6001

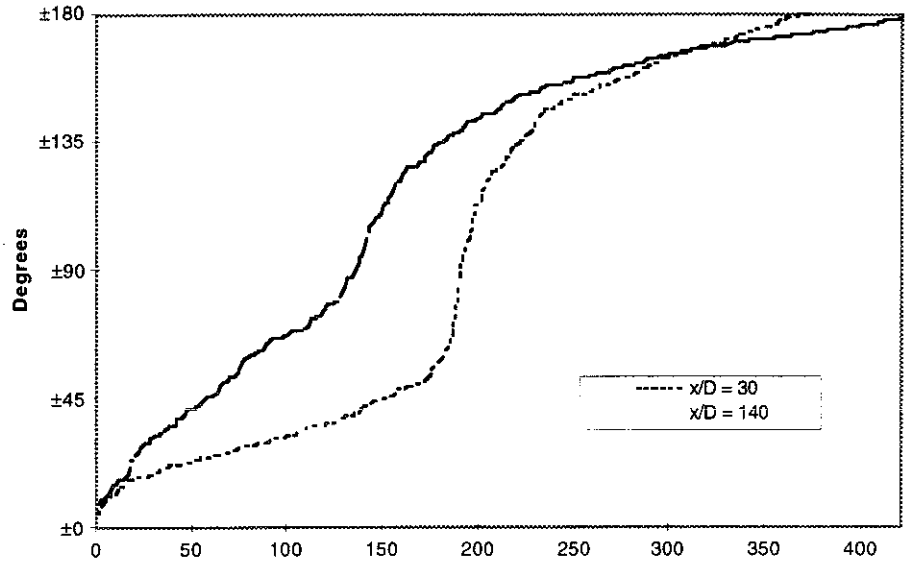

Fig. 6. Number of jets versus orientation.

coincident with the direction of the mean flow, (ii) jets spanning three sensors and with u velocities opposite to the direction of the mean flow, and (iii) two adjacent jets with opposite u velocities spanning two sensors. Deviations of 9°, 18° and 27° in the direction of all vectors in the 3×3 frame for cases (i) and (ii), and in the 2×3 frame for case (iii) have been allowed for in the analysis. Table 2 shows that jets are an additional significant class of structures present in the fully turbulent wake flow, with class (iii) being the dominant jet flow configuration both in the near and far wake regions. For any of the three deviations considered between the vectors in a frame the number of jets (iii) diminishes with x/D, suggesting that some of them have become CEs or ACEs due to the stretching mechanism explained above. These preliminary results suggest that jet motions could explain the genesis and evolution of the double-roller structures or adjacent CE and a ACE in the far wake region.[1,2,5,11,13]

Figure 6 shows the distribution of the number of jet-like motions of types (i) and (ii) with misalignments of 18° as a function of the positive and negative orientation of the u fluctuation. In the near wake most of the jets are either forward (±45°) or backward (180 ± 45°) fluctuating motions with respect to the x-direction, with a similar number of structures in each group. In the far wake turbulence randomises the direction of the forward fluctuating jets (positive u velocities). However, the presence of double-rollers with a strong backward jet-like motion in their centre significantly increases the number of backward motions in the wake (negative u velocities), in agreement with the results reported by Ferré *et al.*[13]

5 CONCLUSIONS

A neural network system based on Fuzzy ARTMAP can be successfully applied to recognise coherent structures in the velocity field of a turbulent flow. The analysis of a turbulent wake flow show that there are clockwise eddies, anticlockwise eddies, four types of saddle points, sources, sinks and jet-like motions. The action of stretching causes the number of eddy motions to increase as the wake develops. The formation of these vertical motions seems to be linked to the shearing action caused by jets of opposing direction occurring near the central horizontal plane in the near and far wake regions. Results are consistent with the occurrence of double-rollers in the far wake reported previously. The present neural network based system is capable of extracting valuable structural information and providing a local understanding of turbulence. These are necessary to model the turbulent transport processes of momentum, heat and mass in turbulent flows.

ACKNOWLEDGEMENTS

We give our thanks to Professor R. A. Antonia for providing his experimental data. We also wish to thank Professor Gail Carpenter and Dr Yousif Asfour for their comments on ART. Financial support was provided by DGICYT project PB93-0656-C02-01 and Ajuts a la Recerca-96 URV 9679c.

REFERENCES

1. Townsend, A. A., *The Structure of Turbulent Shear Flow*, 1st edn. Cambridge University Press, Cambridge, 1958.
2. Grant, H. L., The large eddies of turbulent motion. *Journal of Fluid Mechanics*, 1958, **4**, 149–190.
3. Brown, G. L. and Roshko, A., On density effects and large structure in turbulent mixing layers. *J. Fluid Mech.*, 1974, **64**, 775–816.

4. Carpenter, G. A., Grossberg, S., Marcuzon, N., Reinolds, J. H. and Rosen, D. B., Fuzzy ARTMAP: a neural network architecture for incremental supervised learning of analog multidimensional maps. *IEEE Trans. Neural Networks*, 1992, **3**, 698–713.
5. Ferre-Gine, J., Rallo, R., Arenas, A. and Giralt, F., Identification of coherent structures in turbulent shear flows with a FUZZY ARTMAP neural network. *International Journal of Neural Systems*, 1996 (in press).
6. Pons, D., Estudi de les estructures coherents dels fluxos turbulents tipus estela. Doctoral Thesis, Universistat Rovira i Virgili, Tarragona, Spain, 1996.
7. Vernet, A., Kopp, G. A., Ferré, J. A. and Giralt, F., Simultaneous velocity and temperature patterns in the far region of a turbulent cyllinder wake. *ASME J. Fluids Engng*, 1996 (in press).
8. Carpenter, G., Grossberg, S. and Rosen, D., Fuzzy ART: fast stable learning and categorisation of analog patterns by an adaptive resonance system. *Neural Networks*, 1991, **4**, 759–771.
9. Shaw, R., Multilinear algebra and group representations. In *Linear Algebra and Group Representations*. Academic Press, London, 1983.
10. Zhou, Y. and Antonia, R. A., Critical points in a turbulent near wake. *J. Fluid Mech.*, 1994, **275**, 59–81.
11. Giralt, F. and Ferré, J. A., Structure and flow patterns in turbulent wakes. *Physical Fluids A*, 1983, **5**, 1783–1789.
12. Kopp, G., Ferré, J. A. and Giralt, F., Combining pattern recognition and proper orthogonal decomposition for improved identification of the underlying structure in fully developed turbulence. *ASME J. Fluids Engng*, 1996 (submitted).
13. Ferré, J. A., Savill, A. M., Mumford, J. C. and Giralt, F., Three-dimensional large-eddy motions and fine-scale activity in a plane turbulent wake. *J. Fluid Mech.*, 1990, **210**, 371–414.